State estimation of a solar direct steam generation mono-tube cavity receiver using a modified Extended Kalman Filtering scheme

José I. Zapata[a,*]

[a]*Research School of Engineering, Australian National University, Canberra, 0200, Australia*

Abstract

State estimation plays a key role in the development of advanced control strategies for Concentrating Solar Thermal Power (CSP) systems, by providing an estimate of process variables that are otherwise infeasible to measure. The present study proposes a state estimation scheme for a once-through direct steam generation plant, the SG4 steam generation system at the Australian National University. The state estimation scheme is a modified Extended Kalman Filter that computes an estimate of the internal variables of the mono-tube cavity receiver in the SG4 system, from a dynamic non-linear model of the receiver. The proposed scheme augments the capabilities of a Continuous-Direct Extended Kalman filter to deal with the switched nature of the receiver, in order to produce estimates during system start-up, cloud transients and operation of the plant. The estimation process runs at regular sample intervals and happens in two stages, a prediction and a correction stage. The prediction stage uses the receiver model to calculate the evolution of the system and the correction stage modifies the predicted estimate from measurements of the SG4 system. The resulting estimate is a set of internal variables describing the current state of the receiver, termed the state vector. This paper presents a description of the modified Extended Kalman Filter and an evaluation of the scheme using computer simulations and experimental runs in the SG4 system. Simulations and experimental results in this paper show that the filtering scheme improves a receiver state vector estimation purely based on the receiver model and provides estimates of a quality sufficient for closed loop control.

Nomenclature

$\dot{I}_{sol}$ Direct normal irradiation

$\dot{m}_{in}$ Receiver inlet mass flow

P_{in} Receiver inlet pressure

P_{out} Receiver outlet pressure

T_a Ambient temperature

T_{in} Receiver inlet temperature

$\bar{\gamma}$ System mean void fraction of saturated region

h_{out} Specific enthalpy of fluid at receiver tube outlet

L_1 Length of sub-cooled fluid region in receiver tube

L_2 Length of saturated fluid region in receiver tube

P Average pressure in receiver tube

T_{w1} Wall temperature of tube adjacent to sub-cooled fluid region

T_{w2} Wall temperature of tube adjacent to saturated fluid region

T_{w3} Wall temperature of tube adjacent to superheated fluid region

$\boldsymbol{\phi}_k$ Zero-mean white noise added to measurements

$\boldsymbol{\upsilon}_k$ Zero-mean white noise added to process

$\mathbf{H}_k$ Observation matrix

$\mathbf{K}_k$ Kalman Filter gain

$\mathbf{P}_k$ Error covariance matrix

$\mathbf{Q}_k$ Process noise covariance matrix

$\mathbf{R}_k$ Measurement noise covariance matrix

$\hat{\mathbf{x}}_k$ Estimated state vector

$\mathbf{x}_k$ State vector

$\mathbf{y}_k$ Measurement vector

Subscripts

Δt Intermediate (continuous) time between samples

h Numerical integrator time step

$k|k$ Sample time for prediction (left) and correction (right)

k Current sample

t_k Continuous time at sample k

*Corresponding author

Email address: jose.zapata@anu.edu.au (José I. Zapata)

1. Introduction

Modern state-space control strategies incorporate the internal dynamic behaviour of a system to regulate their output, thus providing a performance advantage over classical (PID) control (Franklin et al., 2010). This increase in sophistication requires knowledge of the internal system behaviour, which may not always be accessible with instruments. Concentrating Solar Thermal Power (CSP) technologies face this challenge in pursuit of modern control strategies that improve their efficiency (Camacho et al., 2012).

Kalman filters can compute an estimate of the internal variables of a system, when direct measurement is impractical or not possible (Kailath et al., 2000). This technique has been extended to non-linear systems in a variety of ways, such as Extended Kalman Filters, Unscented Kalman Filters and particle filters (Rawlings and Mayne, 2009). Extended Kalman Filters have been applied to thermal systems (LeBreux et al., 2013; Jonsson et al., 2007) and CSP applications. For example Schlipf et al. (Schlipf et al., 2012) propose an EKF to estimate the state of the evaporator in a Compact Linear Fresnel Reflector system, and use this estimate in a closed loop controller. In the ACUREX field, Gallego and Camacho (Gallego and Camacho, 2012b) use an Unscented Kalman Filter (Julier and Uhlmann, 1997) to estimate the heat transfer profile of the absorber tube across the entire length of a parabolic trough collector from localised measurements of irradiation and temperature, and use this estimate in an adaptive control scheme (Gallego and Camacho, 2012a).

This study addresses the estimation of internal variables in a mono-tube cavity receiver used for direct steam generation (DSG) with a modified Extended Kalman Filtering scheme. The receiver is part of the SG4 steam generation system, a once-through direct steam generation loop powered by a 500 m^2 paraboloidal dish (Lovegrove et al., 2011). A control oriented mathematical model of the receiver developed by Zapata et al. (Zapata et al., 2013) forms the basis for the estimation algorithm. Model inputs correspond to measurements that influence the receiver behaviour: feed-water mass flow, temperature and pressure, direct normal irradiation (DNI), and receiver outlet pressure. The model produces a set of receiver variables, herein the receiver state vector, that describe the internal dynamical behaviour of the two-phase heat exchange in the receiver in real time.

There exist several challenges to develop a filtering scheme: the model is non-linear, switched, numerically stiff, and susceptible to measurement noise and calibration errors. The filtering scheme proposed in this study approaches these challenges by integrating three Continuous-Discrete Extended Kalman Filters (CDEKF) (Jorgensen et al., 2007; Frogerais et al., 2012) with the SG4 receiver model. The filtering scheme switches between CDEKF instances to handle the switched nature of the model, and each instance handles non-linear numerical solution of the model, including model/measurement uncertainty. The state vector can be employed in modern state-space control strategies for the SG4 system (e.g. Zapata, 2015). This paper describes the modified EKF scheme in detail as well as its realisation in the SG4 system. Preliminary results of this work have been presented in (Zapata, 2014).

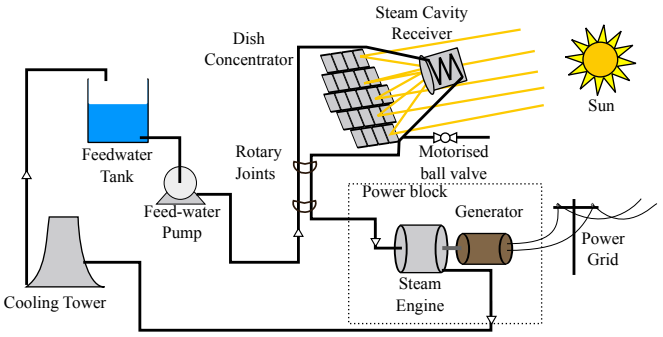

Figure 1: SG4 system diagram with steam engine, from January 2010 to June 2013

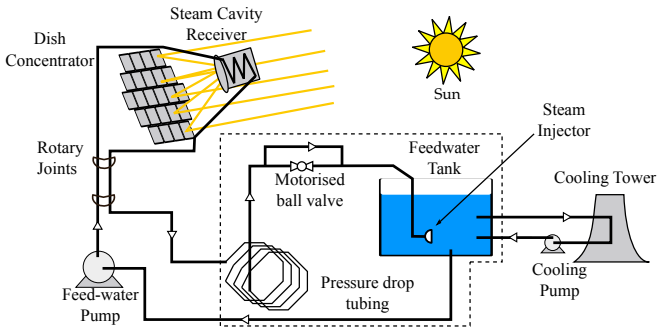

Figure 2: SG4 system diagram with passive dissipation loop, after July 2013

2. The SG4 steam generation system

The SG4 steam generation system is a once-through direct steam generation loop, consisting of a 500 m^2 paraboloidal concentrator, a mono-tube cavity steam receiver, and a hydraulic circuit. The system originally powered a reciprocating steam engine and electrical generator (Fig. 1), but in July 2013 the engine was decommissioned and replaced with a passive back-pressure dissipation loop for safety reasons (Fig. 2). Both configurations have been included because experimental data for section 6 comes from the original configuration and data for section 7 was obtained with the modified configuration.

A Supervisory Control and Data Acquisition (SCADA) system monitors and records experimental data for the SG4 plant. The SG4 system features instruments to measure process variables (e.g. pressure and temperature) and environmental variables (e.g. ambient temperature and direct normal irradiation). The SCADA system samples and stores these measurements at 2 s intervals in a database (Zapata, 2014).

3. State estimation problem

The state estimation problem in this study consists of formulating a scheme to observe the internal dynamics of the SG4 receiver in real time from measurements of the system and a dynamic model of the receiver. The receiver model provides a

fast and accurate representation of the transient heat transfer behaviour in the SG4 system (Zapata et al., 2013). However, the receiver model and measurements are susceptible to noise and calibration errors. This section describes these challenges, and how they steer the choice of a state estimation scheme towards Kalman Filters.

3.1. Switched receiver model

The receiver model provides information about the internal state of the receiver with the following state vector:

$$\mathbf{x} = \begin{bmatrix} L_1 & L_2 & P & h_{out} & \bar{\gamma} & T_{w1} & T_{w2} & T_{w3} \end{bmatrix}^T \quad (1)$$

These variables convey valuable information about the mass inventory in the receiver tube, losses and the steam quality at the receiver outlet. The receiver model is able to predict the onset of two-phase and single phase flow at the outlet due to its ability to switch between three different sets of equations, termed modes. Mode '1' corresponds to liquid at the receiver outlet, mode '1-2' represents saturated water/vapour mixture at the outlet and mode '1-2-3' corresponds to superheated steam. As the model switches between modes, the meaning of some variables in the state vector will change between representing a physical quantity and tracking an initialisation value. A state estimation scheme that uses the receiver model has to either handle the switching nature of the model or be confined to operating on a single mode.

The combined system of equations for each mode is nonlinear and does not have an analytical solution. Therefore, a numerical integration scheme calculates the mode solution and propagates the state vector forward in time. The model is numerically stiff and its solution requires implicit numerical integration schemes (e.g. Kristensen et al., 2004). These aspects of the model also impose restrictions on the state estimation scheme.

3.2. Available input measurements

The receiver model propagates the state vector forward in time when provided with the following set of measurements (i.e. the measurement vector $\mathbf{u}$):

$$\mathbf{u} = \begin{bmatrix} \dot{m}_{in} & P_{in} & P_{out} & T_{in} & T_a & \dot{I}_{sol} \end{bmatrix}^T \quad (2)$$

Measurement error propagates through the receiver model equations and may introduce deviations in the computed estimate. Table 1 summarises the sensitivity of the receiver model to each measurement in vector $\mathbf{u}$. The effect of noise from input measurements on the state vector estimate can be attenuated by a Kalman filtering scheme, if one or more of the states can be observed or measured as well. This condition is called observability, and it determines the number of elements in the state vector of the system (if any) that are observable from its inputs and outputs (Franklin et al., 2010).

Table 1: Measurement uncertainty for experimental data

Measurement	Uncertainty	Model T_{out} sensitivity
$\dot{I}_{sol}$	±20 W/m^2	±33 °C
$\dot{m}_{in}$	±1.1 g/s	±13 °C
P_{in}	±97 kPa	±0.75 °C
P_{out}	±97 kPa	±2 °C
T_{in}	±1 °C	±2 °C
T_a	±0.8 °C	±2 °C
T_{out}	±0.5 °C	N/A
Total sensitivity		±36 °C

3.3. Available output measurements

In addition to the measurements required by the receiver model, it is possible to measure receive outlet fluid temperature T_{out} and pressure P_{out}. These measurements can be used to measure individual variables in the receiver state vector. Pressure state P can be related to measurements at the inlet and outlet of the receiver P_{out} at all times under the model assumption that $P = (P_{in} + P_{out})/2$. The enthalpy state h_{out} can be calculated from steam tables as a function $h_{out} = f(P_{out}, T_{out})$ when the receiver outlet is single phase flow (i.e. modes '1' and '1-2-3'). In mode '1-2' it is not possible to calculate receiver outlet enthalpy, because the flow at the receiver outlet is saturated steam/water mixture, and there was no measurement of steam quality available for this study.

Receiver measurements P_{in}, P_{out} and T_{out} create thus a set of "virtual" output measurements for model states P and h_{out}; but virtual measurements are not consistent across modes. Table 2 summarises the relation between real measurements, "virtual" measurement and receiver vector states, in different receiver model modes.

Table 2: Relation between available output measurements in the SG4 system and receiver model states, for each receiver model mode

State $\mathbf{x}_k$	Measurement $\mathbf{y}_k$		
	Mode '1'	Mode '1-2'	Mode '1-2-3'
L_1	-	-	-
L_2	-	-	-
P	$\frac{1}{2}(P_{in} + P_{out})$	$\frac{1}{2}(P_{in} + P_{out})$	$\frac{1}{2}(P_{in} + P_{out})$
h_{out}	$f^1(P_{out}, T_{out})$	-	$f^{123}(P_{out}, T_{out})$
$\bar{\gamma}$	-	-	-
T_{w1}	-	-	-
T_{w2}	-	-	-
T_{w3}	-	-	-

The observability of the receiver model was tested in this by linearising the model at several operating points across all three receiver modes, and calculating the rank of the resulting observability matrix for each case Åstrom and Murray (2008). This study found that in modes '1' and '1-2-3' the observability matrix of the linearised model is of rank 8, the number of states in the model, and thus the receiver state vector is observable. In mode '1-2' the observer was of rank 5, which limits the choice of state estimators to algorithms that can reconstruct the receiver state over multiple samples, e.g. Kalman Filters.

3.4. Formulating a state estimation scheme

The state estimation scheme needs to handle a switched non-linear model that is susceptible to calibration, noisy and/or inconsistent measurements. Continuous - Discrete Extended Kalman Filters (Frogerais et al., 2012) can handle the non-linear numerical solution to the receiver model, including its susceptibility to measurement and calibration uncertainty. To handle the switched nature of the model and inconsistent output measurements, three separate filters are combined to form the modified Extended Filtering scheme proposed in this study. Section 4 provides a description of CDEKF and section 5 describes the modified Extended Filtering scheme structure in detail.

4. Continuous-Discrete Extended Kalman Filtering

The CDEKF extends the estimation ability of the Kalman filter to continuous-time non-linear systems, and is at the core of the modified Extended Kalman Filtering scheme presented in this study. This section first presents an abridged description of Kalman Filtering to introduce the two-stage estimation process, parameters and notation. Then, the specific characteristics of the CDEKF are introduced.

4.1. The Kalman Filter

The Kalman filter is an optimal estimator widely used to compute an estimate $\hat{\mathbf{x}}_k$ for a linear system state vector $\mathbf{x}_k$ (Kalman, 1960; Grewal and Andrews, 2008). The linear system is of the form:

$$\mathbf{x}_k = \mathbf{F}\mathbf{x}_{k-1} + \mathbf{G}(\mathbf{u}_k + \boldsymbol{\upsilon}_k) \quad (3)$$

$$\mathbf{y}_k = \mathbf{H}\mathbf{x}_k + \boldsymbol{\phi}_k \quad (4)$$

with $\mathbf{F}, \mathbf{G}$ and $\mathbf{H}$ constant matrices and a given initial state vector condition $\mathbf{x}_0$. The system is represented in discrete-time intervals k, due to the sampled nature of input measurements $\mathbf{u}_k$ and output measurements $\mathbf{y}_k$. The system is susceptible to measurement and model uncertainty, and it is represented as additive noise vector signals $\boldsymbol{\upsilon}_k$ and $\boldsymbol{\phi}_k$.

Kalman filters assume that noise signals $\boldsymbol{\upsilon}_k$ and $\boldsymbol{\phi}_k$ are zero mean, uncorrelated white noise disturbances with quantifiable standard deviations. Under this assumption, the uncertainty introduced to the system has expected values, quantified by matrices $\mathbf{Q}_k$ and $\mathbf{R}_k$:

$$\mathbf{Q}_k\delta_{kj} = E\boldsymbol{\upsilon}_k\boldsymbol{\upsilon}_j^T \quad \mathbf{R}_k\delta_{kj} = E\boldsymbol{\phi}_k\boldsymbol{\phi}_j^T \quad (5)$$

where the Kronecker delta is $\delta_{kj} = 1$ for $k = j$ and zero otherwise (Kailath et al., 2000).

The matrix $\mathbf{Q}_k$ is the process covariance matrix and quantifies the uncertainty introduced to equation (3). The matrix $\mathbf{R}_k$ is the measurement covariance and quantifies the uncertainty introduced to equation (4).

The Kalman filter attempts to attenuate the effect of noise in the state estimate by minimising the error vector $\tilde{\mathbf{x}}_k = \mathbf{x}_k - \hat{\mathbf{x}}_k$. From the knowledge of the system and its uncertainty, the error between the state and its estimate $\tilde{\mathbf{x}}_k = \mathbf{x}_k - \hat{\mathbf{x}}_k$ will also have an expected covariance:

$$\mathbf{P}_k\delta_{kj} = E\tilde{\mathbf{x}}\tilde{\mathbf{x}}^T \quad (6)$$

The error covariance matrix $\mathbf{P}_k$ quantifies the accumulated error of the state estimation, and is the metric used by the Kalman filter to minimise the error vector $\tilde{\mathbf{x}}_k$.

At each sample k, the Kalman filter estimation occurs in two steps: a prediction stage and a correction stage.[1] The prediction stage computes a predicted state $\hat{\mathbf{x}}_{k|k-1}$ from the system model equation (3) , previous estimate $\hat{\mathbf{x}}_{k-1} = \hat{\mathbf{x}}_{k-1|k-1}$, and new input samples $\mathbf{u}_k$. The correction stage uses the new output measurement samples $\mathbf{y}_k$ and the predicted state $\hat{\mathbf{x}}_{k|k-1}$ to compute a corrected state $\hat{\mathbf{x}}_{k|k}$, and this becomes the current state estimate $\hat{\mathbf{x}}_k$. The Kalman filter procedure is as follows:

Prediction stage

$$\hat{\mathbf{x}}_{k|k-1} = \mathbf{F}\hat{\mathbf{x}}_{k-1|k-1} + \mathbf{G}\mathbf{u}_k \quad (7)$$

$$\mathbf{P}_{k|k-1} = \mathbf{F}\mathbf{P}_{k-1|k-1}\mathbf{F}^T + \mathbf{G}\mathbf{Q}_k\mathbf{G} \quad (8)$$

Correction stage

$$\bar{\mathbf{e}}_k = \mathbf{y}_k - \mathbf{H}\hat{\mathbf{x}}_{k|k-1} \quad (9)$$

$$\mathbf{K}_k = \mathbf{P}_{k|k-1}\mathbf{H}^T(\mathbf{H}\mathbf{P}_{k|k-1}\mathbf{H}^T + \mathbf{R}_k)^{-1} \quad (10)$$

$$\hat{\mathbf{x}}_{k|k} = \hat{\mathbf{x}}_{k|k-1} + \mathbf{K}_k\bar{\mathbf{e}}_k \quad (11)$$

$$\mathbf{P}_{k|k} = (\mathbf{I} - \mathbf{K}_k\mathbf{H})\mathbf{P}_{k|k-1} \quad (12)$$

Practical implementations of the Kalman filter feature modified calculations that reduce the number of computations and round-off errors (Grewal and Andrews, 2008).

The filter computes a gain matrix $\mathbf{K}_k$ in the correction stage that combines the predicted state $\hat{\mathbf{x}}_{k|k-1}$ with output measurements $\mathbf{y}_k$ in such a way that it minimises the error variance $\mathbf{P}_k = \mathbf{P}_{k|k}$ of the estimate. [2]

4.2. Continuous-Discrete Extended Kalman Filters

The Extended Kalman filter (EKF) employs the Kalman filter to compute a state estimate for non-linear systems by producing a linear approximation of the system using a first order Taylor series expansion (Kailath et al., 2000). The receiver model is numerically stiff and ill-conditioned (Hairer and Wanner, 1999), and a Taylor series approximation yields poor performance for sample times $k > 0.1$ s, and is incompatible with the SG4 system sample time of 2 s.

CDEKF algorithms employ sophisticated numerical integrators to propagate the non-linear system equations and an approximate error covariance matrix between sample times k,

[1] Double subscripts herein indicate prediction p on the left and correction c on the right, i.e. $x_{p|c}$.

[2] The error variance for the instant k depends on the previous estimate $\hat{\mathbf{x}}_{k-1}$ and not on the actual state $\mathbf{x}_k$. Therefore, an adequate initial condition $\hat{\mathbf{x}}_0$ is needed for the success of the estimation.

thus overcoming the numerical limitations of EKF. The literature offers a range of CDEKF algorithms, and the main difference between them is the strategy to numerically propagate the state vector and approximate error covariance (Frogerais et al., 2012).

In general terms, the prediction stage of the CDEKF replaces equations (7) and (8) with

$$\hat{\mathbf{x}}_{k|k-1} = \mathsf{solve1}(t_k, \hat{\mathbf{x}}_{k-1|k-1}, \mathbf{u}_k, \mathbf{f}(\mathbf{x}, \mathbf{u})) \quad (13)$$

$$\mathbf{P}_{k|k-1} = \mathsf{solve2}(t_k, \hat{\mathbf{x}}_{k-1|k-1}, \mathbf{Q}_k, \mathbf{P}_{k-1|k-1}, \mathbf{g}(\mathbf{x}, \mathbf{u})) \quad (14)$$

Where functions solve1 and solve2 are place-holders for the selected numerical algorithms. The filtering scheme procedure in study selected the numerical integrator and approximate error covariance propagator proposed by Jorgensen et al. (Jorgensen et al., 2007) (see section 5.1), due to its numerical stability and fast computational performance. The functions proposed by Mazzoni (Mazzoni, 2008) were also trialled in this study; they exhibited good numerical stability, but exhibited higher computation times and thus were not employed for the results in the paper.

The relation between states and outputs is no longer the matrix $\mathbf{H}$ but the non-linear function $\mathbf{y} = \mathbf{g}(\mathbf{x}, \mathbf{u})$, the CDEKF algorithm also modifies the Kalman filter correction equation (9) with:

$$\bar{\mathbf{e}}_k = \mathbf{y}_k - \mathbf{H}_k \hat{\mathbf{x}}_{k|k-1} \text{ where } \mathbf{H}_k = \left.\frac{\partial \mathbf{g}}{\partial \mathbf{x}}\right|_{\hat{\mathbf{x}}_{k|k-1}} \quad (15)$$

It is possible to solve numerically at each time step k if an analytical solution is not possible.

5. A modified Extended Kalman Filtering Scheme for the SG4 receiver

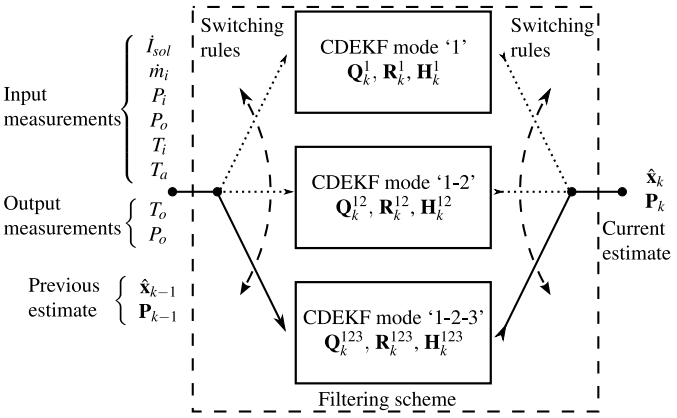

Figure 3: Diagram of the modified Extended Kalman Filter presented in this study. Solid arrows represent the flow of variables in the active mode and dotted arrows for inactive modes

This study solves the state estimation problem in section 3 with a modified Extended Kalman Filtering scheme. The filtering scheme combines the SG4 receiver model in (Zapata et al., 2013) with a set of Continuous - Discrete Extended Kalman Filters (CDEKF), to compute an estimated receiver state vector. The filtering scheme can be viewed as an augmented state estimator composed of three independent CDEKF filters running concurrently with the model, with one model mode and corresponding CDEKF filter active at any given time (Fig. 3). The filtering scheme thus switches between the same modes as the receiver model, according to the same rules, and tailors the estimation process accordingly. In addition, the filtering scheme resets the error covariance matrix at switching for consistency in the error estimation. Each CDEKF filter is tuned independently to produce the best possible estimation for the active mode.

This section outlines the filtering scheme procedure, the strategy to switch and engage different model modes, the considerations to tune the CDEKF filter for each mode, and numerical considerations for the filtering scheme as a whole.

5.1. Filtering scheme procedure

The filtering scheme procedure follows the prediction and correction stages of the CDEKF, but can switch model modes and filter parameters in continuous time (i.e. between samples k) during the prediction stage (step 2(d)). It is this modification to the CDEKF procedure that allows the filtering scheme to cover the entire range of operating conditions represented by the receiver model. The CDEKF algorithm in (Jorgensen et al., 2007) propagates the square root of the error covariance matrix, to guard against numerical round-off errors.[3] Hence, the exponent $^{1/2}$ herein denotes the *matrix square root* operator.

The filtering scheme procedure is as follows:

1. Require $\hat{\mathbf{x}}_{k-1|k-1}$, $\mathbf{P}^{1/2}_{k-1|k-1}$, t_k, $\mathbf{Q}^{1/2}_k$, $\mathbf{R}^{1/2}_k$, $\mathbf{y}_k$, and receiver mode.
2. Prediction stage. Start at $\Delta t = h$
   (a) Calculate intermediate model predicted state $\hat{\mathbf{x}}_{\Delta t|k-1}$ with the solve1 function, i.e. the implicit Runge-Kutta integrator in (Jorgensen et al., 2007)
   (b) Calculate intermediate error covariance $\mathbf{P}^{1/2}_{\Delta t|k-1}$ using the solve2 function, i.e. the approximate covariance algorithm in (Jorgensen et al., 2007)
   (c) Adjust integration step h based on integrator error convergence
   (d) Evaluate switching conditions. If required, switch model mode and filter (see sec. 5.2)
   (e) Increment $\Delta t = \Delta t + h$ and repeat from 2(a) until $\Delta t = t_k$
   (f) Return $\hat{\mathbf{x}}_{k|k-1} = \hat{\mathbf{x}}_{t_k|k-1}$ and $\mathbf{P}^{1/2}_{k|k-1} = \mathbf{P}^{1/2}_{t_k|k-1}$
3. Correction stage
   (a) Compute approximated model output $\mathbf{H}_k = \left.\frac{\partial \mathbf{g}}{\partial \mathbf{x}}\right|_{\hat{\mathbf{x}}_{k|k-1}}$
   (b) Compute measurement error $\bar{\mathbf{e}} = \mathbf{y}_k - \mathbf{H}_k \hat{\mathbf{x}}_{k|k-1}$

[3] In particular to preserve its positive semi-definiteness (Kailath et al., 2000).

(c) Compute filtering gains $\mathbf{K}_k$

(d) Compute corrected estimate $\hat{\mathbf{x}}_{k|k}$ and refresh error covariance matrix $\mathbf{P}_{k|k}^{1/2}$

4. Repeat for next time step t_{k+1}

5.2. Switching between filters

Switching enables the filtering scheme to fully exploit the ability of the receiver model to describe different flow patterns in the receiver tube.

For the filtering scheme, the check for switching conditions occurs at step 2(d) of the algorithm procedure. During this step, the switching rules evaluate the intermediate state estimate $\hat{\mathbf{x}}_{\Delta t|k-1}$ and its time derivative $\hat{\dot{\mathbf{x}}}_{\Delta t|k-1}$ employing the same rules that trigger switching in the receiver model (see Zapata et al., 2013).

If the filtering scheme detects when a switching condition occurs, it proceeds to:

1. Store the intermediate state vector $\hat{\mathbf{x}}_{\Delta t|k-1}$ in memory
2. Switch receiver model modes
3. Replace CDEKF matrices $\mathbf{Q}_k$, $\mathbf{R}_k$ and $\mathbf{H}_k$ with the corresponding matrices for new the mode
4. Reinitialise the error covariance matrix $\mathbf{P}_{\Delta t|k}$
5. Resume the prediction stage with the active CDEKF settings and $\hat{\mathbf{x}}_{\Delta t|k-1}$ as the initial condition

The filtering scheme must substitute the parameters of the prediction and correction stages of the CDEKF, so that the estimation process is consistent with the behaviour of the model. All filtering scheme parameters (see section 5.4) are tuned from knowledge of the SG4 system, receiver and filtering scheme simulations.

Switching also reinitialises the error covariance matrix, to prevent the filtering process from using information from an inactive mode, as shown next.

5.3. Reinitialisation of intermediate error covariance matrix at switching times

The filtering scheme updates the intermediate error covariance matrix $\mathbf{P}_{\Delta t|k-1}$ at each integration step Δt of the prediction stage. Model switching affects the filtering scheme because state variables change meaning between modes, and this poses a mismatch with the information accrued in the error covariance matrix.

State variables can either be physical or *inactive*. Physical states obey the mass and energy balance equations established for the active receiver mode. *Inactive* states pertain the description of an inactive flow region in the receiver model and follow convenient initialisation values. For each mode in the receiver model, the set of physical and *inactive* state variables is:

Mode '1' Physical states: P, h_{out} and T_{w1}; *inactive* states L_1, L_2, $\bar{\gamma}$, T_{w2} and T_{w3}.

Mode '1-2' Physical states: L_1, P, h_{out}, $\bar{\gamma}$, T_{w1} and T_{w2}; *inactive* states: L_2 and T_{w3}.

Mode '1-2-3' Physical states L_1, L_2, P, h_{out}, $\bar{\gamma}$, T_{w1}, T_{w2} and T_{w3}; *inactive* states: none.

If the information accrued by the error covariance matrix about a physical state variable is used to correct an *inactive* state variable (or vice versa), the filtering scheme can apply an erroneous correction to the state and cause the algorithm to diverge. For example, early filtering scheme simulations revealed that when the filtering scheme switches from mode '1-2-3' to '1-2' the information in the covariance matrix caused the correction stage to incorrectly adjust L_2, which caused $L_1 + L_2 > L$. When the model switched back to mode '1-2-3', $L_3 = L - L_1 - L_2 < 0$ which is physically meaningless and caused the simulation to diverge.

This study tried two different approaches to deal with the mismatch between the error covariance matrix and the receiver mode at switching times: re-initialising the covariance matrix and keeping three separate covariance matrices, one for each mode.

Re-initialisation of the covariance matrix consists of overwriting the covariance matrix a diagonal matrix whose non-zero elements are arbitrarily small (e.g. $\epsilon = 10^{-3}$). Initialising the filter with a small error covariance matrix is a common practice (Dhaouadi et al., 1991; Plett, 2004; Frogerais et al., 2012, e.g) and it biases initial estimates towards the predicted state vector (i.e. a small filter gain $\mathbf{K}_k$).

Maintaining separate error covariance matrices keeps three matrices in memory i.e. $\mathbf{P}_k^1$, $\mathbf{P}_k^{12}$ and $\mathbf{P}_k^{123}$. At the start of the estimation process, the filtering scheme initialises all three matrices as arbitrarily small (see above) and selects the error covariance matrix corresponding to the active mode, e.g. $\mathbf{P}_k^1$ for mode '1'. The filtering scheme updates this covariance matrix until step 2(d) triggers a mode switch. From then on, the filtering scheme replaces the error covariance matrix with the corresponding matrix for the new mode (e.g. $\mathbf{P}_k^{12}$ for mode '1-2') but keeps the previous error covariance matrix in memory. When the observer switches back to a previously used mode, it uses the stored covariance matrix for that mode and so forth.

Simulations of the filtering scheme showed no difference in performance between approaches. For simplicity, results in this study use the first approach of reinitialising the error covariance matrix as arbitrarily small at switching times.

5.4. Tuning the filtering scheme response

Each filtering scheme mode m uses three matrices to tune the response of its corresponding filter: a process error covariance matrix $\mathbf{Q}_k^m$, a measurement error covariance matrix $\mathbf{R}_k^m$ and an observation matrix $\mathbf{H}_k^m$. The coefficients assigned to each matrix in each mode influence the computation of the filter gain $\mathbf{K}_k$, and together these matrices calibrate the filtering scheme response (see Table 3).

5.4.1. Process error covariance matrix

For each mode m, the process covariance matrix $\mathbf{Q}_k^m$ assigns an expected uncertainty to the prediction stage, and the result-

Table 3: Filtering scheme parameter matrices for all modes

Matrix	Value
$\mathbf{Q}_k^1$	$\text{diag}\{0, 0, 3, 50, 0, 2, 0, 0\}$
$\mathbf{R}_k^1$	$\begin{pmatrix} 3 & 0 \\ 0 & 50 \end{pmatrix}$
$\mathbf{H}_k^1$	$\begin{pmatrix} 0 & 0 & 1 & 0 & 0 & 0 & 0 & 0 \\ 0 & 0 & 0 & 0 & 0 & 0 & 0 & 0 \end{pmatrix}$
$\mathbf{Q}_k^{12}$	$\text{diag}\{0.1, 0, 3, 100, 0.01, 2, 2, 0\}$
$\mathbf{R}_k^{12}$	$\begin{pmatrix} 3 & 0 \\ 0 & 50 \end{pmatrix}$
$\mathbf{H}_k^{12}$	$\begin{pmatrix} 0 & 0 & 1 & 0 & 0 & 0 & 0 & 0 \\ 0 & 0 & 0 & 0 & 0 & 0 & 0 & 0 \end{pmatrix}$
$\mathbf{Q}_k^{123}$	$\text{diag}\{1, 0.5, 3, 150, 0.01, 2, 2, 5\}$
$\mathbf{R}_k^{123}$	$\begin{pmatrix} 3 & 0 \\ 0 & 50 \end{pmatrix}$
$\mathbf{H}_k^{123}$	$\begin{pmatrix} 0 & 0 & 1 & 0 & 0 & 0 & 0 & 0 \\ 0 & 0 & 0 & 1 & 0 & 0 & 0 & 0 \end{pmatrix}$

ing state vector $\hat{\mathbf{x}}_{k|k-1}$. Three factors condition the expected uncertainty of the state prediction: the inherently approximated nature of the receiver model, errors introduced by noisy input measurements to the model (e.g. DNI or mass flow), and the meaning (i.e. physical or *inactive*) of each state in the active mode m. When the meaning of a state is physical, its expected uncertainty will reflect how the model uncertainty and input measurement noise propagates through the receiver model.

When a state is *inactive* it has zero uncertainty so that the correction stage of the filtering scheme does not interfere with the receiver model propagation of *inactive* states. In both cases, the expected uncertainty of each state corresponds to a coefficient in the diagonal of matrix $\mathbf{Q}_k^m$ (in the same order as the state vector variables in eq. (3)). Non-diagonal coefficients in matrix $\mathbf{Q}_k^m$ represent the cross covariance between states, and are also set to zero in the absence of statistical information about the system. Table 3 summarises the coefficients for matrix $\mathbf{Q}_k^m$ employed in this study. These coefficients were chosen from knowledge of the system and simulation trials. Note, for example, that diagonal coefficients for the process covariance matrix $\mathbf{Q}_k^{123}$ are all non zero, consistent with all state variables having a physical meaning in the prediction stage. States that already had a physical meaning in modes '1' and '1-2' have greater variances in this mode, as early trials showed that this enhanced the performance of the filtering scheme. In particular, this enhanced the filtering scheme ability to reject large spikes in measurements (see section 6).

5.4.2. Measurement error covariance matrix

The measurement error covariance matrix $\mathbf{R}_k^m$ informs the filtering scheme on the expected uncertainty in output measurements. Output measurement uncertainty comes from noise, instrument precision and their calibration, which is the same across all filtering scheme modes.

The diagonal coefficients in measurement covariance matrices $\mathbf{R}_k^m$ correspond to the expected uncertainty in "virtual" measurements of average receiver pressure P and outlet enthalpy h_{out}. "Virtual" measurement uncertainties depend on the variance of real measurements P_{in}, P_{out} and T_{out} (see Table 1).

Table 4: Numerical integrator parameters for the filtering scheme

Parameter	Value
relative tolerance	1×10^{-2}
absolute tolerance	1×10^{-4}
iteration tolerance	1×10^{-1}
h_{min} simulations	1×10^{-1} s
h_{max} simulations	2 s
h_{min} experiments	5×10^{-3} s
h_{max} experiments	5×10^{-1} s

Average receiver pressure in the receiver model is defined as $P = P_{in}/2 + P_{out}/2$, thus the variance for its measurement is $\sigma_P^2 = \sigma_{P_{in}}^2/2 + \sigma_{P_{out}}^2/2$. Outlet enthalpy is a function of measurements P_{out} and T_{out} from steam property tables, and the variance of "virtual" measurement h_{out} is the maximum deviation that propagates through the steam table function, i.e.

$$\sigma_{h_{out}}^2 = \left[\sup f(P_{out} \pm \sigma_{P_{out}}, T_{out} \pm \sigma_{T_{out}}) - \inf f(P_{out} \pm \sigma_{P_{out}}, T_{out} \pm \sigma_{T_{out}})\right]^2 \quad (16)$$

For the SG4 system, $\sigma_P^2 \approx 1\,\text{bar}^2$ and $\sigma_{h_{out}}^2 \approx [25, 50]\ \text{kJ}^2/\text{kg}^2$, depending on the combination of pressure and temperature fed to steam tables. This study assigns conservative variance coefficients, i.e. higher uncertainties to measurements.

5.4.3. Observation matrix

Observation matrices $\mathbf{H}_k^m$ map output measurements to state vector variables, to asses the estimation error. Due to the preprocessing of real output measurements into "virtual" measurements (see previous section) the observation matrices $\mathbf{H}_k^m$ simplify to linear matrices and there is no need to compute a linear approximation as shown in eq. (15). However, there is an inconsistency between modes as to which "virtual" measurements are available to the correction stage.

It is possible to use both pressure and enthalpy measurements when the fluid exits the receiver as single phase. But it is only possible to use "virtual" measurement P when the fluid at the outlet is saturated, as there is no steam quality measurement in the SG4 system. Furthermore, early filtering scheme simulations show that the enthalpy measurement h_{out} prevents the filter to switch from mode '1' to mode '1-2' as the estimated enthalpy $\hat{h}_{out}$ tends to follow the value of saturated liquid enthalpy h_f. Therefore, this study uses only "virtual" measurements of pressure P for modes '1' and '1-2', and both P and h_{out} measurements for mode '1-2-3' (see Table 3).

5.5. Tuning the numerical integrator

During the prediction stage, the filtering scheme uses the ESDIRK34 numerical integrator (Kristensen et al., 2004) to propagate the solution of the receiver model forward in time. The numerical integrator performs iterative calculations of the receiver model and its Jacobian matrix to reach a solution at each time step, and a variable integration step size h to manage

the stability and computational cost of the solution. The filtering scheme performance depends on the relative and absolute tolerances of the iteration loop, the Jacobian matrix calculation method, and the management of integration step size h. Table 4 shows the parameters employed in this study.

The filtering scheme calculates the Jacobian matrix of the receiver model numerically, using a pre-conditioned backward difference method (Brenan et al., 1996). During simulation trials, a forward difference method exhibited numerical instability and a central difference scheme showed comparable performance to the backward scheme, at additional computation cost.

The filtering scheme manages the integration step size h by evaluating the error convergence monitor of the ESDIRK34 integrator. If the error converge monitor reports non-convergence, the filtering scheme halves h and repeats the integration step. If $h = h_{min}$, the filtering scheme accepts the solution, to prevent the algorithm from going beyond the numerical precision of the implementation hardware. An adequately tuned value of h_{min} (see table 1) minimises the possibility of solution divergence, performs with stability over extended periods (see section 5). When the error convergence monitor reports converges, the filtering scheme increases h by h_{min} and continues. This basic integration step size management balances the numerical stability and computational cost of the filtering scheme and exhibits typical time steps of $h \approx 10h_{min}$.[4]

6. Simulated performance of the filtering scheme

The filtering scheme was implemented in simulations to evaluate is ability to estimate the state of the SG4 receiver. This section presents two simulations of the SG4 system. The first simulation employs the receiver model in (Zapata et al., 2013) to compute the system state, in order to establish a baseline performance for the filtering scheme. The second simulation employs the full filtering scheme to compute the receiver state, and demonstrates how the correction introduced by the filtering scheme aids the state estimation. The output of both simulations is shown in Figs. 4 and 5.

6.1. Implementation

The filtering scheme was implemented using GNU Octave, an open source package with advanced matrix and vector operation capabilities (Eaton, 2001). GNU Octave also features a C++ application programming interface (API), which enabled the deployment of the filtering scheme in the experimental SG4 system (see section 7). The receiver model in (Zapata et al., 2013) was re-implemented in GNU Octave from FORTRAN without modifications, to constitute the prediction stage of the filtering scheme. The simulated filtering scheme employs the XSteam routine (Holmgren, 2007), to calculate water properties. Simulations read SG4 system measurements and filter parameters from text files, performed all computations in the filtering scheme procedure (see section 5.1) and wrote state estimations into text data files for analysis. All simulations ran on a 64-bit personal computer.

[4]The time step management strategy employed in (Kristensen et al., 2004) was also trialled in this study, but exhibited worse performance in simulations.

Table 5: Parameters for receiver model in filtering scheme

Item	Value	Item	Value
L	212 m	U_1^1	25 W/(m^2 K)
L_{min}	1 m	U_1^{12}	25 W/(m^2 K)
h_{min}	10 kJ/kg	U_1^{123}	25 W/(m^2 K)
D_i	0.02 m	U_2^{12}	11.25 W/(m^2 K)
D_o	0.026 m	U_2^{123}	22.5 W/(m^2 K)
c_w	460 J/(kg K)	U_3^{123}	12.5 W/(m^2 K)
ρ_w	9700 kg/m^3	G_1^1	0.13
τ	7.07 mN/m^2	G_1^{12}	0.14
ϵ	0.87	G_1^{123}	0.15
$\tau_{\tilde{\gamma}}$,τ_T	35 1/h	G_2^{12}	0.12
α_1	2500 W/(m^2 K)	G_2^{123}	0.13
α_2	5166 W/(m^2 K)	G_3^{123}	0.065
α_3	860 W/(m^2 K)		

6.2. Input data for simulations

An experimental run of the SG4 system provides data for the simulations in this section. The run occurred on the 22nd of January 2013 with the original system configuration (see fig 1). During the experimental run, the SG4 concentrator tracked the sun while maintaining approximately constant feed-water flow for approximately 2.5 h. The fluid at the receiver outlet transitioned from liquid water to superheated steam and produced steam for approximately 2 h. The steam engine came online at approximately 0.4 h into the run, causing a sharp increase in pressures along the line. The experimental run concluded when cloud cover prevented operation for the remainder of that day.

This data was selected because it includes a start-up transient in the receiver response as well as a significant measurement error: a short malfunction in the feed-water flow measurement at 2.25 h. The start-up transient allows simulations to demonstrate how the filtering scheme switches modes, and the measurement errors demonstrate how the filtering scheme attenuates noise.

Simulations also require: a set of receiver model parameters, numerical integration parameters, and a set of filter tuning parameters. Receiver model parameters correspond to the values listed in Table 5 except for concentrator conditions (average concentrator reflectivity r =80 % and effective aperture area A_{eff} = 470 m^2), which vary between runs. The numerical integrator parameters correspond to values in Table 4 and filter parameters correspond to values in Table 3.

6.3. Simulation results

Figs. 4(a) and 5(a) show measured DNI for the experimental run employed in simulations. The signal is zero at times when the SG4 dish concentrator was not tracking the sun. Measured DNI exhibits two brief drops at approximately 1.8 h and 2.25 h caused by high altitude wispy clouds, and drastic changes from approximately 2.3 h caused by the onset of permanent cloud cover.

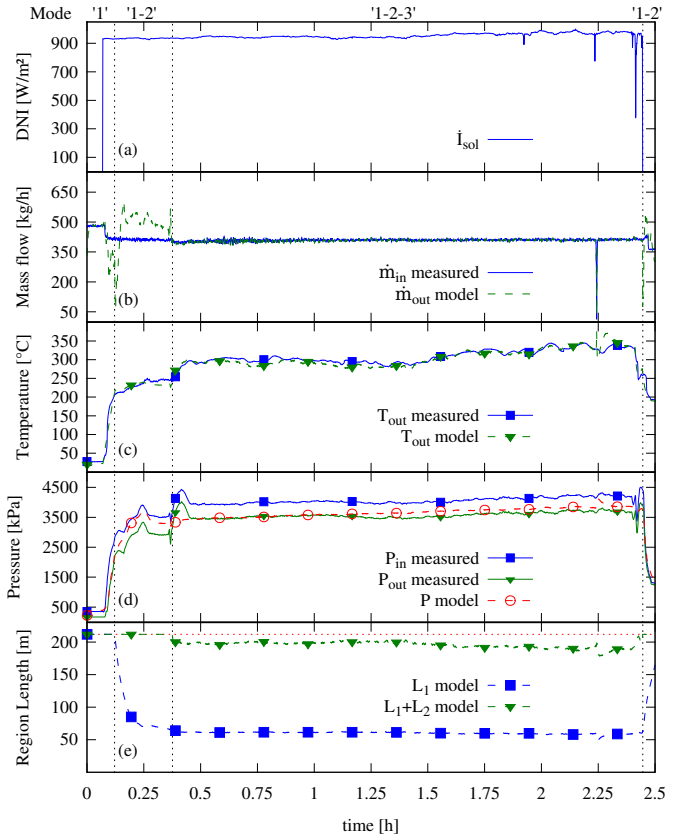

Figure 4: Filtering scheme simulation with model-only prediction and SG4 experimental data. Measured (–), simulated (- -). Vertical dotted lines indicate mode switching. (a) DNI. (b) Feed-water and outlet mass flow. (c) Receiver outlet temperature. (d) Inlet, outlet and average receiver pressure. (e) Cumulative length of fluid regions, with respect to tube length (horizontal dotted line).

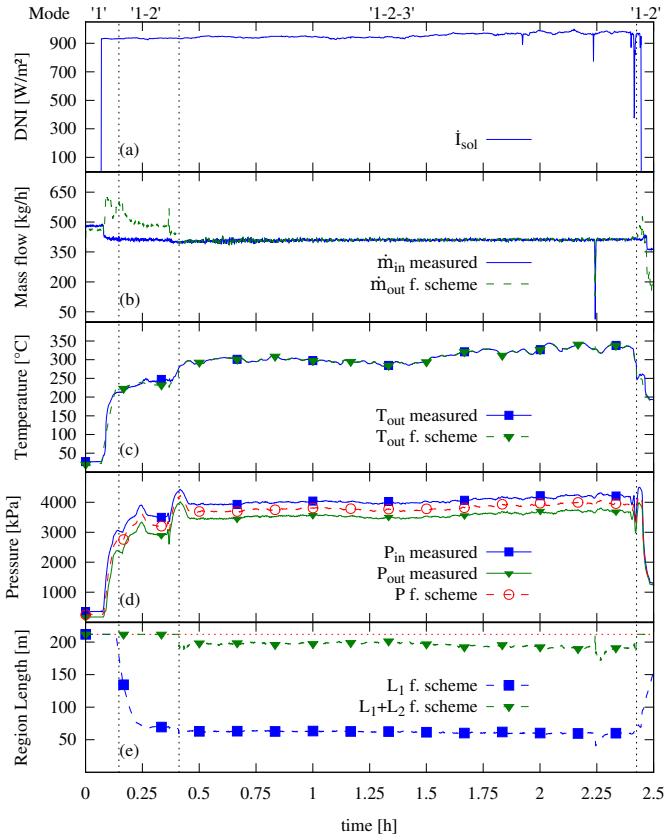

Figure 5: Filtering scheme simulation with full scheme prediction/correction and SG4 experimental data. Measured (–), simulated (- -). Vertical dotted lines indicate mode switching. (a) DNI. (b) Feed-water and outlet mass flow. (c) Receiver outlet temperature. (d) Inlet, outlet and average receiver pressure. (e) Cumulative length of fluid regions, with respect to tube length (horizontal dotted line).

Panel (b) in Figs. 4 and 5 show receiver outlet mass flows computed by the model and the filtering scheme respectively, alongside measured feed-water mass flow $\dot{m}_{in}$. The feed-water mass flow was set to a constant value throughout the run, except at the start of the run to protect the receiver from thermal shock. Mass flow measurements exhibit moderate noise throughout the run and a sharp drop at approximately 2.25 h, caused by a temporary malfunction in the flow sensor. The outlet mass flow computed by filtering scheme in Fig. 5(b) differs from the model estimate during the start-up transient, as the computed pressure estimate differs between model-only and filtering scheme results.

The temperature estimate generated by the receiver model, shown in Fig. 4(c), shows good agreement with measured temperatures during the run, but is susceptible to noise in mass flow and DNI measurements. In comparison, the temperature estimate of the filtering scheme in Fig. 5(c) shows better agreement than model-only results, including the rejection of a disturbance caused by a sharp drop in mass flow measurements at approximately 2.25 h.

Average receiver pressure P as computed by the receiver model (Fig. 4(d)) shows fair agreement with pressure measurements, except during large pressure transients during the experimental run. A large pressure transient occurs at 0.35 h, when the SG4 steam system directs steam from the receiver to the engine instead of the cooling tower. Model simplifications sacrifice pressure P agreement during such transients, to preserve agreement with outlet temperatures (Zapata et al., 2013). On the other hand, the filtering scheme receiver pressure $\hat{P}$ estimate (Fig. 5(d)) stays between measurements P_{in} and P_{out} at all times.

Flow regions computed by model-only and filtering scheme simulations behave similarly (panel (e) of figs. 4 and 5). In both simulations region lengths vary in length according to mass inventory changes in the receiver tube, and as modes switch. The filtering scheme however, switches to mode '1-2-3' approximately 90 s later and then returns to mode '1-2' approximately 60 s earlier than the model-only simulation. The filtering scheme switching times depend on the trajectory of pressure estimates $\hat{P}$, which differ from model-only pressure calculations. Flow region lengths computed by the filtering scheme are also more sensitive to the mass flow measurement error at 2.25 h. Fig. 6 in page 10 zooms into this transient, to compare the model-only and filtering scheme responses.

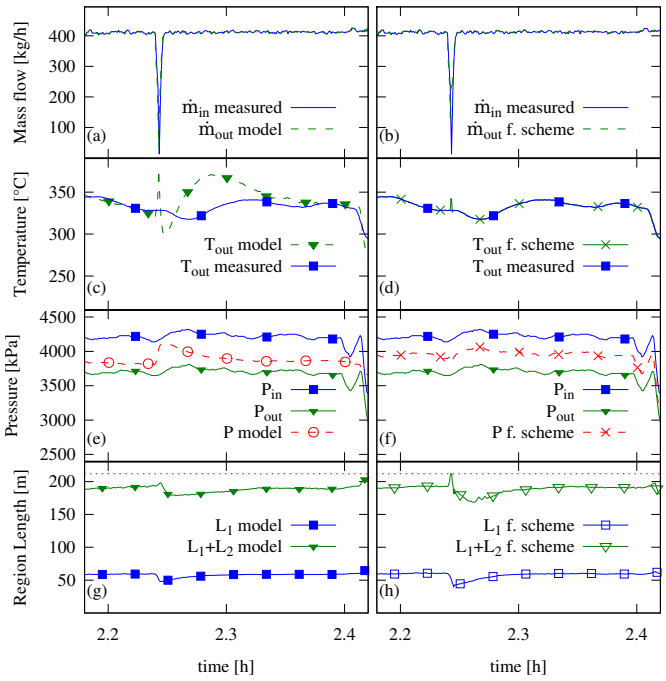

Figure 6: Detailed view of mass flow measurement disturbance around t=2.25 h in model-only (left hand panels) and full filtering scheme (right hand panels) simulations, with SG4 experimental data. (a) Model-only mass flows. (b) Full filtering scheme mass flows. (c) Model-only receiver outlet temperature. (d) Full filtering scheme receiver outlet temperature. (e) Model-only receiver pressure, with inlet and outlet pressures. (f) Filtering scheme receiver pressure, with inlet and outlet pressures. (g) Model-only length of fluid regions and (h) Filtering scheme length of fluid regions with respect to tube length (horizontal dotted line).

6.4. *Filtering scheme performance during mass flow measurement error*

The simulated filtering scheme (Fig. 5) overcomes the error introduced by uncertainty using the information provided by "virtual" measurements P and h_{out}. Although the prediction stage of the filtering scheme is susceptible to the same bias as model-only calculations, the initial condition for each model prediction is the corrected state $\hat{\mathbf{x}}_{k|k}$, which has been adjusted from measurements. Fig. 6 shows model-only and filtering scheme simulations side by side to compare their behaviour when the mass flow sensor disturbance occurs.

Receiver outlet temperatures are shown in Figs. 6(c) and 6(d). The model-only simulation follows measured temperatures closely, until the disturbance in feed-water flow measurement happens at 2.25 h. The receiver model interprets the drop in $\dot{m}_{in}$ as an energy and mass balance transient in the absorber tube, and this results in a spike and subsequent transient in modelled T_{out}. By contrast, the filtering scheme exhibits a moderate spike, and the transient is suppressed.

The filtering scheme attenuates the effect of the mass flow measurement error on the receiver pressure estimate $\hat{P}$. Fig. 6(e) shows a fluctuation on model-only receiver pressure caused by the false drop in mass flow. In contrast, Fig. 6(f) shows how the filtering scheme attenuates the pressure disturbance and closely follows virtual measurement $P = P_{in}/2 + P_{out}/2$.

The correction stage of the filtering scheme affects all variables in the state vector, even if they are not related to available measurements. For example fluid region lengths L_1 and L_2, shown in Figs. 8(g) and 8(h). In both model-only and filtering scheme simulations, fluid region lengths show a transient fluctuation at the time of the mass flow measurement disturbance. However, region lengths vary more drastically in the full filtering scheme than in model-only simulations. The filtering scheme gain $\mathbf{K}_k$ applies a correction across all state vector variables during the mass flow measurement disturbance, introducing greater variation to region length estimates. This arises from the trade-off encountered when tuning the filter with the parameters employed in the simulation.

6.5. *Parameter influence on filtering scheme simulations*

The performance of the filtering scheme depends on the tuning of all its parameters: model calibration, covariance matrices $\mathbf{Q}_k$ and $\mathbf{R}_k$, and numerical integration parameters.

Tuning the filtering scheme depends strongly on the calibration of the receiver model. It is possible to tune filtering scheme to run with worse model calibrations, by increasing the magnitude of coefficients in process covariance matrices $\mathbf{Q}_k$. In effect, larger coefficients in $\mathbf{Q}_k$ assign greater uncertainty to input measurements and how they propagate through the receiver model. But tuning the filtering scheme to deal with greater model uncertainty leads to an increase in the accumulated error in $\mathbf{P}_k$, and thus to greater correction to estimates. Large correction estimates can cause the filter to diverge, if it leads to a violation of the physical constraints of the receiver model (e.g. it may make fluid region lengths violate the condition $L_1 + L_2 + L_3 = L$). Therefore, it is best to ensure an adequate model calibration and then select the smallest coefficients in matrices $\mathbf{Q}_k$ that provide an acceptable performance for the filtering scheme (see section 5.4 for details).

The amount of allowable calibration error for each parameter in the receiver model depends on its influence on the model response. Experience with the SG4 system suggests that the main source of uncertainty is the current conditions of the concentrator surface, characterised by reflectivity r and effective receiver aperture A_{eff}. An increase in average concentrator reflectivity r from 84 % to 85 % results in an increase of approximately 4.7 kW in incoming power. The increase changes state variables by up to 2% while other inputs are maintained constant. Other model parameters (see Table 5) both exert less influence on the model and tend not to vary, so they may remain at their initial calibration values.

Measurement covariance matrices $\mathbf{R}_k$ account for the uncertainty in "virtual" measurements P and h_{out} and thus depend on the precision of measurements P_{in}, P_{out} and T_{out} (see section 5.4). Although it is possible to alter the filtering scheme performance by varying the coefficients in matrices $\mathbf{R}_k$, it is recommended that they only reflect instrument precision to avoid overcorrection to the state vector estimate.

Filtering scheme simulations are more sensitive to numerical integration parameters than model-only simulations. In particular, full scheme simulations require a minimum integration step $h_{min} = 0.1$ s (see Table 4) to perform adequately across

a range of data sets, whereas model-only simulations produce good results with $h_{min} = 0.5$ s. Filtering scheme simulations incur additional calculations to propagate the error covariance matrix $\mathbf{P}_k$, and this increases the chances of numerical instability caused by round-off errors (Grewal and Andrews, 2008). This study takes a conservative approach to tune the numerical parameters of the filtering scheme, preferring numerical stability over computational cost.

7. Experimental performance of the filtering scheme in the SG4 system

The filtering scheme was implemented in the SG4 system to evaluate its ability to compute a state vector for the SG4 receiver in real time. Experimental results confirm that the filtering scheme performs as predicted by simulations in the SG4 system.

7.1. Experimental filtering scheme implementation

The experimental filtering scheme employed the same code as simulations in section 6; modified to exchange data with the SG4 SCADA system in real time at 2 s intervals during operation. Experimental filtering scheme parameters were identical to simulations, except for concentrator conditions and numerical integration step size. Measurements carried out on the 8th of October 2013 determined an average concentrator reflectivity $r = (86.2 \pm 0.5)\,\%$ to account for soiling, and an effective aperture $A_{eff} = 460\,\mathrm{m}^2$ to account for damaged mirror panels. Numerical integration step size bounds h_{min} and h_{max} used in experiments were smaller than simulations, as early runs of the experimental filtering scheme suffered from numerical instability and/or diverged. Early run data was re-simulated offline, but the simulated filtering scheme did not exhibit numerical problems. One possibility for this difference is that simulations were compiled and run in a 64-bit processor using Ubuntu Linux, whereas experimental runs were executed in a Windows 7 personal computer and built using a 32-bit MinGW tool-kit. Despite this difference, acceptable numerical performance was attained by the experimental filtering scheme by using smaller integration step size bounds (see Table 4). The experimental filtering scheme executes one iteration of the scheme procedure in section 5.1, in approximately 25 ms.

7.2. Experimental run data

The results in this section, shown in Fig. 7, correspond to an experimental run of the SG4 system conducted on the 11th of October 2013, for approximately 4 h. Ambient conditions consisted of clear skies and ambient temperatures ranging from 15 °C to 20 °C. The SG4 system configuration was the post July 2013 (Fig. 2), where steam travels through a back-pressure pipe network instead of driving a reciprocating steam engine. The back-pressure pipe network maintained receiver pressures ranging from 3 MPa to 4 MPa, comparable to experimental runs with the steam engine (c.f. experimental data for Figs. 4 and 5). The SG4 system operated for 30 min before the experimental run, which preheated the receiver and caused a faster than typical start-up time.

Fig. 7(a) shows the measured DNI during the experimental run. A discrete "on-sun" signal modulates DNI measurements to indicate the moments in the run when the SG4 concentrator starts and stops tracking the sun.

Feed-water mass flow Fig. 7(b) exhibit high frequency oscillations at flows below 350 g/s (i.e. in the first two hours of the run). The cause of these oscillations is not known, but as they do not result in receiver outlet temperature variations, it is conjectured to be a form of sensor/measurement noise.

Initially, a high flow was set to protect the receiver preheating section while the concentrator moves to track the sun. Subsequently, feed-water flows were changed at incremental steps by the operator to obtain receiver outlet temperatures of 520 °C, 460 °C and 400 °C during the run. At each steady state, receiver temperatures exhibited small fluctuations attributed to oscillations in DNI.

7.3. Experimental filtering scheme results

The filtering scheme produced receiver outlet temperature estimates that agree well with measurements, in particular when the receiver outlet is superheated (see Fig. 7(c)). This agreement occurs despite the noise in feed-water flow measurements, which demonstrates the ability of the filtering scheme to attenuate noise in estimates. In mode '1-2' measured and estimated receiver outlet temperatures do not agree during start-up, but they do so during cool-down. The start-up transient is examined in more detail in section 7.3.1.

Receiver pressure estimates behave as predicted by simulations. Fig. 7(d) shows that throughout the entire experimental run, estimated receiver pressures stayed half way between measurements of inlet and outlet receiver pressure.

Estimated region lengths in Fig. 7(e) reflect the change in mass inventory in the absorber tube as the filtering scheme transitions between modes '1', '1-2' and '1-2-3'. During the start-up transient, the filtering scheme estimates the movement of region boundaries as regions become active and occupy the length of the absorber tube. Later in the run, the filtering scheme estimated subtler changes in region lengths as the SG4 system operated at different mass flow settings. At the end of the run, region lengths show the reverse mode transition from mode '1-2-3' to modes '1-2' and mode '1' at the end of the experimental run, consistent with the predicted behaviour of the filtering scheme in simulations.

7.3.1. Experimental filtering scheme performance during the start-up transient

Receiver outlet temperatures in Fig. 7(c) show that during the start-up period, the filtering scheme disagrees with temperature measurements while in mode '1-2'. Steam at the receiver outlet reached a superheated condition approximately 5 min after the SG4 dish started to track the sun for this run.

This start-up time is 3 times faster than typical, and it is due to a false system start that preheated the receiver before the experimental run. In the SG4 system, it typically takes approximately 15 min for receiver outlet temperatures to reach superheat once the dish starts to track the sun (c.f. data in Fig. 4).

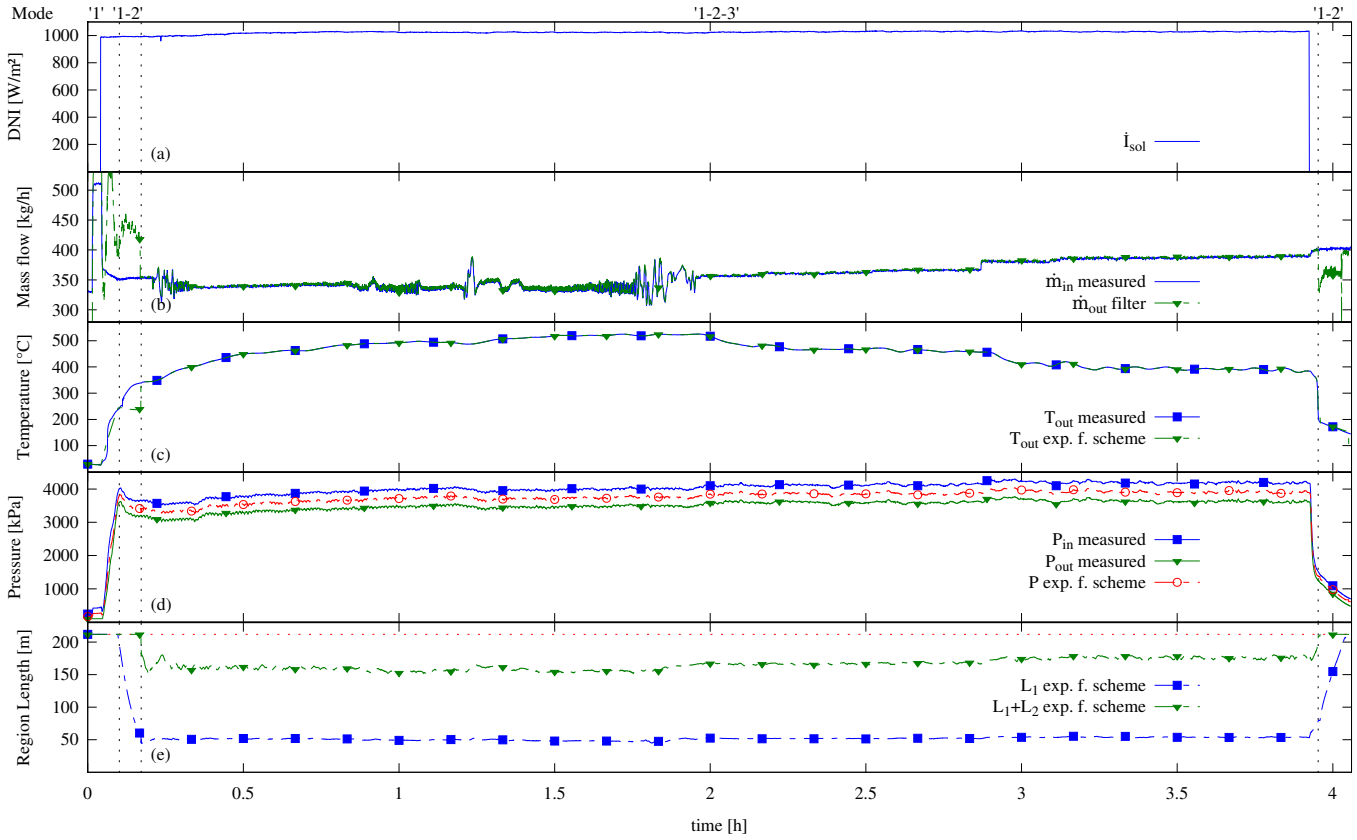

Figure 7: Experimental results of the filtering scheme, calculated simultaneously with an experimental run on 11th of October 2013. Measured (–), experimental (– - -). Vertical dotted lines indicate mode switching. (a) DNI. (b) Feed-water and outlet mass flow. (c) Receiver outlet temperature. (d) Inlet, outlet and average receiver pressure. (e) Cumulative length of fluid regions, respect to tube length (horizontal dotted line).

The filtering scheme prediction did not account for the receiver preheating and therefore underestimated the rate of increase in outlet enthalpy during the start-up transient.

The filtering scheme did follow the progression from liquid, to saturated and then to superheated steam at the outlet, eventually recovering from this mismatch. Once in mode '1-2-3', the filtering scheme corrected the state estimate thanks to the additional "virtual" measurement of receiver outlet enthalpy h_{out}, and showed agreement to less than 0.5 °C with outlet receiver temperatures, even under fast fluctuations in measured feed-water flow (Fig. 7(b)).

This slow start-up estimation was repeated in simulations of the filtering scheme, confirming that this phenomenon is a limitation of the receiver model and not an experimental implementation issue.

7.3.2. *Experimental filtering scheme performance at steady operating periods*

Fig. 8 shows the performance of the filtering scheme at an intermediate period in the experimental run from 2.5 h to 3.5 h. In this portion of the run, the SG4 system responded to incremental increases in feed-water mass flow and fluctuations in DNI.

Feed-water mass flows, shown in Fig. 8(b), were changed in step increments to lower the receiver outlet temperature from 460 °C to 400 °C, with the largest step increment at approximately 2.88 h. This mass flow increment also caused a slight increase in system pressures, as shown in Fig. 8(d). DNI, shown in Fig. 8(a), remained at approximately $(1030 \pm 5)\,\mathrm{W/m^2}$ and oscillated with a period of approximately 7 min. The SG4 dish concentrator converted the DNI oscillation into concentrator power fluctuations of approximately ±2 kW.

The experimental filtering scheme responded to these fluctuations and maintained close agreement with measurements. Measured and estimated temperatures in Fig. 8(c) agree to less than 0.5 °C and the filtering scheme reproduces both transient and oscillatory fluctuations in temperature. The estimated receiver pressure $\hat{P}$ in Fig. 8(d) tracks pressure fluctuations caused by both DNI oscillation and step increases in mass flow.

Estimated flow region lengths respond to changes in mass flow and oscillations in DNI. Fig. 8(e) shows that the length of the estimated saturation region $\hat{L}_2$ grew after the step increase in feed-water flow. At higher flows, the fluid obtains less heat per unit mass from the absorber tube and thus travels further along the tube length to reach superheated conditions. Additionally, both region boundaries exhibit small oscillations due to the influence of DNI fluctuation on the energy and mass balances in the absorber tube.

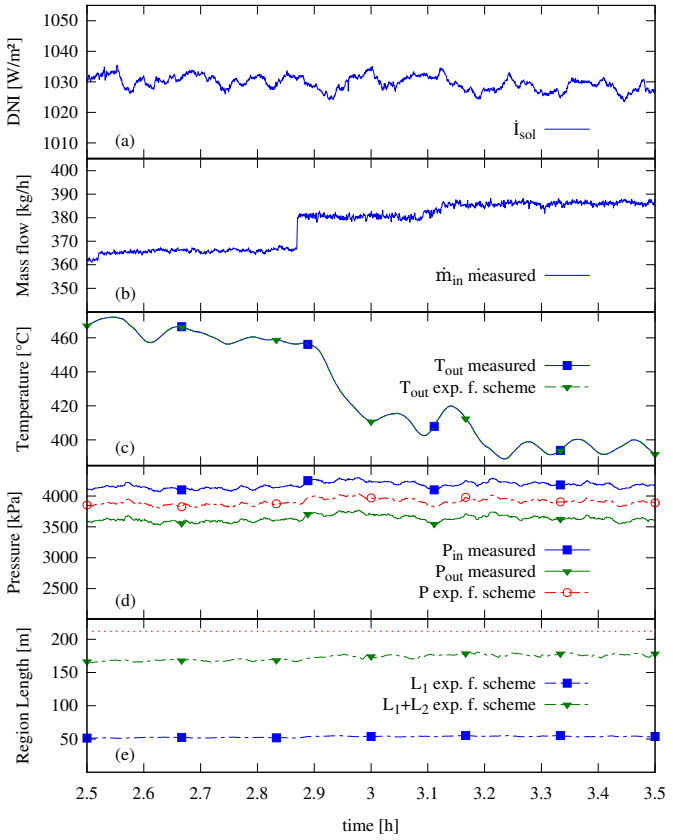

Figure 8: Experimental results of the filtering scheme, calculated simultaneously with an experimental run on 11th of October 2013; intermediate operation period. Measured (–), experimental (– - -). Vertical dotted lines indicate mode switching. (a) DNI. (b) Feed-water and outlet mass flow. (c) Receiver outlet temperature. (d) Inlet, outlet and average receiver pressure. (e) Cumulative length of fluid regions, respect to tube length (horizontal dotted line).

8. Conclusion

The filtering scheme proposed in this paper combines the state-space description of the SG4 receiver in (Zapata et al., 2013) with the estimation ability of Continuous-Discrete Extended Kalman Filtering, to provide a robust estimation of the mono-tube cavity receiver state vector. The filtering scheme handles the switched nature of the receiver model and the inconsistency of available output measurements to correct the state vector estimate. The scheme runs three separate CDEKF filters and switches between them depending on the trajectory of state estimates. Each filter possesses its own set of tuning parameters, and it is tailored to work with the active receiver mode and corresponding available measurements. The computed state vector estimate describes the internal state of the SG4 receiver, with tolerance to uncertainty in both the receiver model and measurements.

Simulations in section 6 showed that the filtering scheme improves the model-only estimation of the receiver state vector thanks to the corrective action of available measurements. In particular, estimated receiver outlet temperatures in mode '1-2-3' show very good agreement with measurements when compared with model-only estimates. The filtering scheme uses measurements of receiver pressures P_{in}, P_{out} and outlet temperature T_{out} to correct the estimate of average receiver pressure $\hat{P}$ and receiver outlet enthalpy $\hat{h}_{out}$.

Simulations also revealed that the filtering scheme has a limited ability to correct for model uncertainty, and it benefits from adequate parameter tuning. Adequate parameter calibration can easily be established by obtaining good agreement between model-only simulations and experimental measurements. Out of all receiver model parameters, average reflectivity r and effective aperture area A_{eff} are both the most likely parameters to vary, and the ones with the largest influence over the receiver model.

Experimental results show the successful implementation of the filtering scheme in the SG4 steam generation system. The filtering scheme ran concurrently with the operation of the SG4 system, obtained measurements from the SCADA and computed state estimates at regular intervals. Numerical stability issues with initial trials in the experimental scheme can be managed by reducing the numerical integration step size and tuning the software compilation process.

The estimates produced by the filtering scheme proposed in this study are suitable for the development modern state-space based control schemes to regulate the temperature at the outlet of the SG4 receiver.

9. Acknowledgements

The author wishes to acknowledge the insightful comments provided by Dr. Jochen Trumpf to develop the theoretical part of this study, and the assistance of Mr. Greg Burgess for experimental development and testing. This work has been supported by the Australian Renewable Energy Agency (ARENA).

References

Åstrom, K.J., Murray, R.M., 2008. Feedback Systems. Princeto University Press.

Brenan, K., Campbell, S.L., Petzold, L., 1996. Numerical Solution of Initial-Value Problems in Differential-Algebraic Equations. second ed., SIAM, Philadelphia.

Camacho, E., Berenguel, M., Rubio, F., Martinez, D., 2012. Control of Solar Energy Systems. Springer.

Dhaouadi, R., Mohan, N., Norum, L., 1991. Design and implementation of an extended Kalman filter for the state estimation of a permanent magnet synchronous motor. Power Electronics, IEEE Transactions on 6, 491–497. doi:10.1109/63.85891.

Eaton, J.W., 2001. Octave: Past, present, and future, in: DSC 2001 Proceedings of the 2nd International Workshop on Distributed Statistical Computing.

Franklin, G.F., Powell, J.D., Emami-Naeini, A., 2010. Feedback Control of Dynamics Systems. 6th ed., Upper Saddle River [N.J.]: Pearson.

Frogerais, P., Bellanger, J.J., Senhadji, L., 2012. Various ways to compute the continuous-discrete extended Kalman filter. Automatic Control, IEEE Transactions on 57, 1000 –1004. doi:10.1109/TAC.2011.2168129.

Gallego, A., Camacho, E., 2012a. Adaptative state-space model predictive control of a parabolic-trough field. Control Engineering Practice 20, 904 – 911. doi:10.1016/j.conengprac.2012.05.010.

Gallego, A., Camacho, E., 2012b. Estimation of effective solar irradiation using an unscented Kalman filter in a parabolic-trough field. Solar Energy 86, 3512 – 3518. doi:10.1016/j.solener.2011.11.012.

Grewal, M., Andrews, A., 2008. Kalman Filtering: Theory and Practice using MATLAB. Wiley-IEEE Press.

Hairer, E., Wanner, G., 1999. Stiff differential equations solved by Radau methods. Journal of Computational and Applied Mathematics 111, 93 – 111. doi:http://dx.doi.org/10.1016/S0377-0427(99)00134-X.

Holmgren, M., 2007. Freeware IF97 properties for water and steam. www.x-eng.com. Accessed June 2009.

Jonsson, G.R., Lalot, S., Palsson, O.P., Desmet, B., 2007. Use of extended Kalman filtering in detecting fouling in heat exchangers. International Journal of Heat and Mass Transfer 50, 2643 – 2655. doi:10.1016/j.ijheatmasstransfer.2006.11.025.

Jorgensen, J., Thomsen, P., Madsen, H., Kristensen, M., 2007. A computationally efficient and robust implementation of the continuous-discrete extended Kalman filter, in: American Control Conference, 2007. ACC '07, pp. 3706 –3712. doi:10.1109/ACC.2007.4282549.

Julier, S.J., Uhlmann, J.K., 1997. New extension of the Kalman filter to nonlinear systems, in: AeroSense'97, International Society for Optics and Photonics. pp. 182–193.

Kailath, T., Sayed, A.H., Hassibi, B., 2000. Linear Estimation. Prentice Hall New Jersey.

Kalman, R.E., 1960. A new approach to linear filtering and prediction problems. Transactions of the ASME–Journal of Basic Engineering 82, 35–45.

Kristensen, M.R., Jørgensen, J.B., Thomsen, P.G., Jørgensen, S.B., 2004. An esdirk method with sensitivity analysis capabilities. Computers & Chemical Engineering 28, 2695 – 2707. doi:10.1016/j.compchemeng.2004.08.004.

LeBreux, M., Désilets, M., Lacroix, M., 2013. An unscented Kalman filter inverse heat transfer method for the prediction of the ledge thickness inside high-temperature metallurgical reactors. International Journal of Heat and Mass Transfer 57, 265 – 273. doi:10.1016/j.ijheatmasstransfer.2012.10.036.

Lovegrove, K., Burgess, G., Pye, J., 2011. A new 500 m2 paraboloidal dish solar concentrator. Solar Energy 85, 620 – 626. doi:DOI:10.1016/j.solener.2010.01.009.

Mazzoni, T., 2008. Computational aspects of continuous–discrete extended Kalman-filtering. Computational Statistics 23, 519–539. doi:10.1007/s00180-007-0094-4.

Plett, G.L., 2004. Extended Kalman filtering for battery management systems of LiPb-based HEV battery packs: Part 1. background. Journal of Power Sources 134, 252 – 261. doi:http://dx.doi.org/10.1016/j.jpowsour.2004.02.031.

Rawlings, J.B., Mayne, D.Q., 2009. Model predictive control: Theory and design. Nob Hill Publishing.

Schlipf, D., Hanel, L., Maier, H., 2012. Model based controller design for a steam drum in linear fresnel CSP-plant using direct evaporation, in: Proceedings of the 18th SolarPACES Conference, Marrakech, Morocco.

Zapata, J., 2014. A modified extended Kalman filter to estimate the state of the SG4 receiver at the Australian National University, in: Proceedings of the 52nd Annual Conference of the Australian Solar Council, Melbourne, Australia.

Zapata, J., 2015. Full state feedback control of steam temperature in a once-thorough direct steam generation receiver powered by a paraboloidal dish. Journal of Solar Energy Engineering 137, 0210171–10.

Zapata, J.I., Pye, J., Lovegrove, K., 2013. A transient model for the heat exchange in a solar thermal once through cavity receiver. Solar Energy 93, 280 – 293. doi:10.1016/j.solener.2013.04.005.